NJC

RSC Publishing

PAPER

View Article Online
View Journal

Published on 01 May 2013. Downloaded by Fudan University on 31/05/2013 12:55:02.

Cite this: DOI: 10.1039/c3nj00186e

The reaction of *NH*-indazoles with 1-fluoro-2,4-dinitrobenzene: the unusual formation of benzotriazole-*N*-oxides†‡

Ibon Alkorta,*[a] Fernando P. Cossío,[b] José Elguero,[a] Nieves Fresno,[a] Laura Hernandez-Folgado,[a] Santiago García-Granda,[c] Laura Menéndez-Taboada,[c] Ruth Pérez-Fernández,[a] Felipe Reviriego[a] and Lucia Vázquez-Viñuela[c]

Received (in Montpellier, France)
18th February 2013,
Accepted 30th April 2013

DOI: 10.1039/c3nj00186e

www.rsc.org/njc

When *N*-unsubstituted indazoles, like indazole itself, reacted with 1-fluoro-2,4-dinitrobenzene or 1-chloro-2,4,6-trinitrobenzene, three products were obtained whose structures were determined by X-ray diffraction. Besides the two *N*-substituted nitroaryl derivatives, a third compound was obtained with the same molecular formula ($C_{13}H_8N_4O_4$) to which was assigned the structure of a derivative of benzotriazole *N*-oxide. With the combined use of crystallography, NMR and DFT calculations this reaction was studied with special stress on the mechanism of formation of the benzotriazole-*N*-oxide.

Introduction

Many years ago, some of us reported an unprecedented reaction between *NH*-indazoles and 1-halo-2-nitrobenzenes, such as 1-fluoro-2,4-dinitrobenzene (**2**) and 1-chloro-2,4,6-trinitrobenzene (picryl chloride).[1,2] In Fig. 1 are reported the results obtained in the first case, using three conditions, reflux in ethanol (10 min), reflux in xylene (60 h) and fusion. The percentages vary from one experiment to the other, here are the values obtained in the first case: 29% of **3**, 62% of **4** and 9% of **5**.

NH-Indazoles such as indazole itself **1** and 7-methylindazole exist as a mixture of two tautomers, **a** and **b**, but the 1*H*-tautomer **a** is largely predominant.[3–5] When reacting **1** with 1-fluoro-2,4-dinitrobenzene (**2**) three products were isolated: the 1-dinitrophenyl derivative **3**, which is not formed, for obvious steric reasons, when there is a methyl group at the 7-position; the 2-dinitrophenyl derivative **4**, and a third isomer **5**.[1] The compounds were tentatively identified by ^{1}H NMR[1] and, in the case of **5**, by the $^1J(^1H–^{13}C)$ of the formyl group (185 Hz).[2] The results obtained with 1-chloro-2,4,6-trinitrobenzene were similar.

To explain the formation of the benzotriazole *N*-oxide **5** we proposed the following mechanism (Fig. 2).[2] It was based on general knowledge but without any experimental proof.

It involves the minor 2*H*-tautomer **1b** but according to the Gustafsson paradox,[3,6–10] the less stable tautomer **1b** should be the most reactive. A 1,3-dipolar cycloaddition of the *o*-nitro group on the 1-azadiene moiety of 2*H*-indazole **1b** affords **6** that followed by a nucleophilic substitution of the fluorine atom yields **7**. A [2+2+2] retrocycloaddition would transform **7** into the azo–nitroso derivative **8**, an intermediate in the synthesis of benzotriazole *N*-oxides such as **5** (usually not isolated in the reduction of an azo–nitro derivative).[11,12]

We decided to study again the reaction of indazole **1** with 1-fluoro-2,4-dinitrobenzene (**2**) yielding **3**, **4** and **5** with the following purposes:

(i) To verify the structure of these compounds in the solid state (X-ray crystallography).

(ii) To carry out GIAO/DFT calculations to determine, by comparison with NMR chemical shifts, some aspects of their structure.

(iii) To search for a mechanism for the reaction **1** + **2** → **5** to be more consistent with present day knowledge.

Results and discussion

Since we have conserved the reaction crude of 1967, we carried out the separation of the three isomers ($C_{13}H_8N_4O_4$) using column chromatography (dichloromethane/hexane/methanol).

[a] *Instituto de Química Médica, C.S.I.C., Juan de la Cierva, 3, E-28006 Madrid, Spain. E-mail: ibon@iqm.csic.es*
[b] *Departamento de Química Orgánica I, Kimika Fakultatea, Universidad del País Vasco – Euskal Herriko Unibertsitatea, Manuel de Lardizabal 3, 20018 San Sebastián-Donostia, Spain*
[c] *Departamento de Química Física y Analítica, Facultad de Química, Universidad de Oviedo-CINN, E-33006 Oviedo, Spain*

† Dedicated to Professor Alan R. Katritzky on the occasion of his 85th birthday.

‡ Electronic supplementary information (ESI) available: General experimental methods; ^{1}H and ^{13}C NMR spectra; electronic spectra; computational data. CCDC 806879, 806880, 806881 and 923952. For ESI and crystallographic data in CIF or other electronic format see DOI: 10.1039/c3nj00186e

Published on 01 May 2013. Downloaded by Fudan University on 31/05/2013 12:55:02.

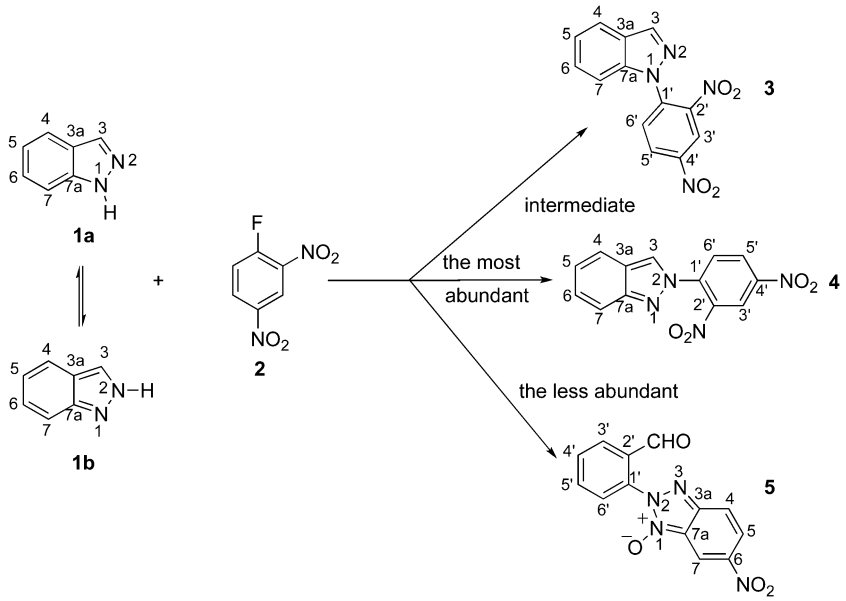

Fig. 1 The 1967–1968 results (under the three conditions the relative abundances were similar).

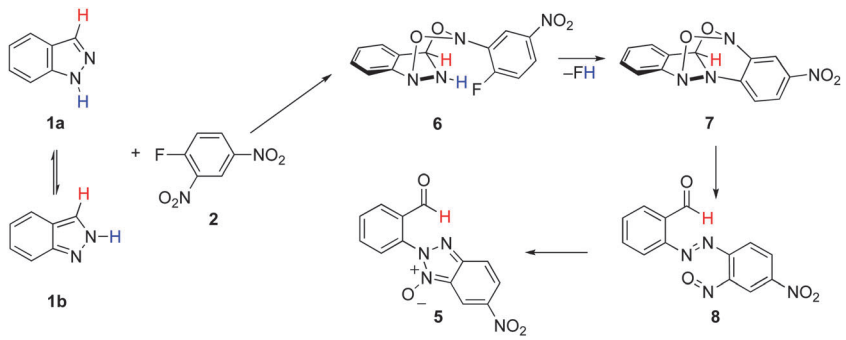

Fig. 2 The 1968 proposed mechanism of the formation of benzotriazole *N*-oxide **5**.

A fourth product was isolated: the hemiacetal of **5**, a rather unstable compound that is irrelevant for the problem under study (in 1967 we used fractional crystallization). We were fortunate to obtain suitable single crystals of **3**, **4** and **5**.

Part I: structure and the mechanism of formation of the 1-(2,4-dinitrophenyl)-1*H*-indazole (3) and 2-(2,4-dinitrophenyl)-2*H*-indazole (4)

Crystallography. The structures of **3** and **4** display no noticeable modifications in crystal packing at different temperatures. Both compounds form parallel chains to the *bc* plane, the molecules forming the chains are linked by H-bonds. In both cases, there are weak intramolecular interactions. For compound **3**, the structure at room temperature does not present changes with that derived from low temperature data, except for a higher structure expansion due to higher atomic displacements.

Crystal structure of 3. The structure is represented in Fig. 3. The 3D structure is formed by chains parallel to the *bc* plane (Fig. 4). In these chains the molecules are linked by hydrogen bonds C–H···O between the oxygen atoms of the nitro group

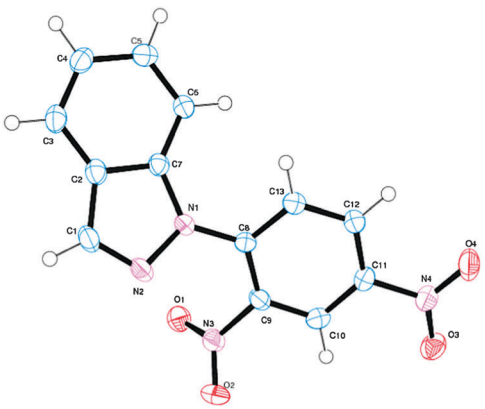

Fig. 3 A view of **3** with displacement ellipsoids drawn at the 50% probability level. The numbering does not follow the systematic one.

N(4) of one molecule, O(3) and O(4), and the phenyl carbons of the other molecule, C(12) and C(13). The O(4) forms a hydrogen bond with C(6) of the indazole benzene ring.

 This journal is © The Royal Society of Chemistry and the Centre National de la Recherche Scientifique 2013

Published on 01 May 2013. Downloaded by Fudan University on 31/05/2013 12:55:02.

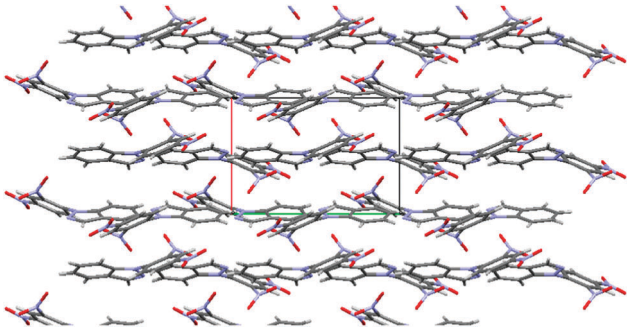

Fig. 4 View of the layers along the *bc* plane of **3**.

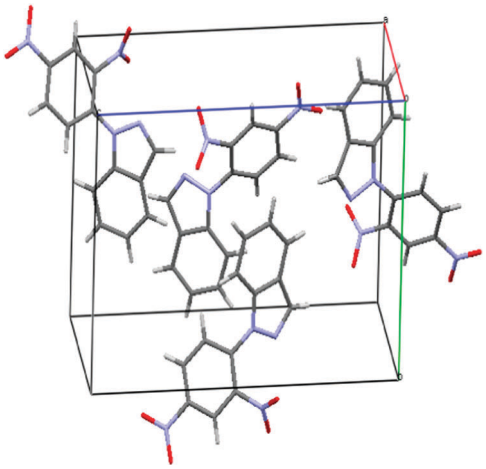

Fig. 5 Packing diagram of **3**.

There are intramolecular interactions between N(2) and N(3) which fix the orientation of the N(3) nitro group. The distance between N(2) and N(3) is 2.765(2) while N(2) and O(1) is 2.834(2) Å. The chains are supported by weak C–H···O hydrogen bonds between the oxygen atoms of both nitro groups and the phenyl carbons of the other molecule, without noticeable strong interactions located (Fig. 5).

Crystal structure of ***4.*** The asymmetric unit of 2-(2,4-dinitrophenyl)-2*H*-indazole is a dimer (Fig. 6). There are intramolecular interactions between N(1) and N(3) stabilizing the orientation of the N(3) nitro group in both molecules of the dimer, with distances 2.739(3) and 2.737(3) Å respectively. The distances between N(1) and O(1) are 2.881(3) Å for molecule A, and 2.828(2) Å for molecule B.

The molecules of the dimer are linked by C9B–H9B···O1A hydrogen bonds and by π–π stacking interactions, with centroid–centroid distances of 3.804(1) and 3.709(1) Å (Fig. 7). The crystal packing is formed by chains parallel to the *bc* plane. In these chains the molecules are linked by weak hydrogen bonds C–H···O between the oxygen atoms of both nitro groups and the benzene CHs of the other molecule along the *b* axis (C2B–H2B···O4B, C7B–H7B···O2B, C9B–H9B···O2B) (Fig. 8). The hydrogen bonds of structures **3** and **4** are listed in Table 7.

Optimized *vs.* experimental geometries. Calculations were carried out at the B3LYP/6-311++G(d,p) level. For structures **3** and **4** we have started with geometries where the nitro group is on the same side as the "pyridine-like" nitrogen atom of the indazole ring (the so-called "orthogonal interaction").[13] Then, we found that the calculated chemical shifts (next section) were consistent with the experimental values in the case of **3** but not in the case of **4**. Therefore, we calculated the opposite conformation (**4′**) finding that it was slightly more stable than **4** (0.7 kJ mol^{-1}) and subsequently we used this conformation for the NMR calculations. Remember that the X-ray structure of the 2-dinitrophenyl derivative, above discussed, has the **4** or *Z* conformation.

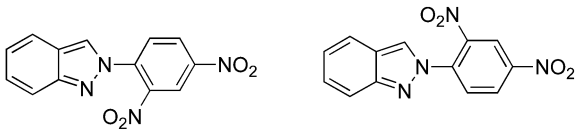

4 **4′**

The bond lengths and bond angles are similar for the experimental and calculated geometries of **3** and **4′**. Table 1 reports the torsion angles (in °) that show only small differences.

NMR spectroscopy and GIAO/DFT calculations. The chemical shifts of both dinitrophenyl indazoles (see Experimental section) are reported in Table 2 together with the chemical shifts calculated at the GIAO//B3LYP/6-311++G(d,p) level (see Computational details).

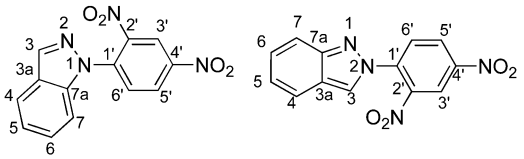

3 **4′**

We have transformed the absolute shieldings (σ, ppm) into chemical shifts (δ, ppm) using the two empirical equations we have established previously:

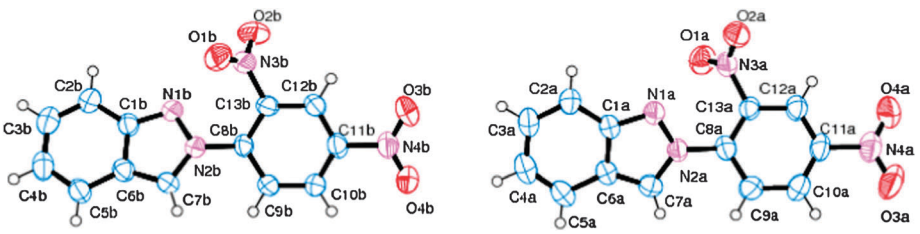

Fig. 6 A view of **4** at 120 K with displacement ellipsoids drawn at the 50% probability level. The numbering does not follow the systematic one.

Published on 01 May 2013. Downloaded by Fudan University on 31/05/2013 12:55:02.

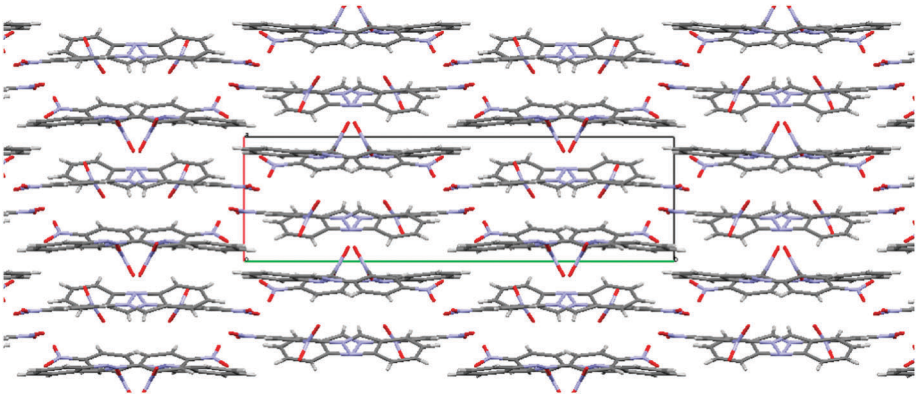

Fig. 7 View of the layers along the *bc* plane of **4** at 120 K.

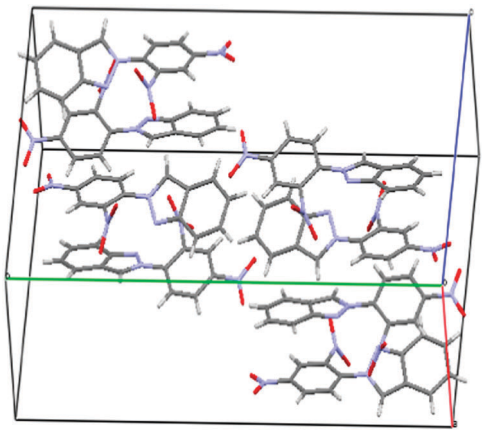

Fig. 8 Packing diagram of **4** at 120 K.

$$\delta^{1}\mathrm{H} = 31.0 - 0.97\sigma^{1}\mathrm{H}\ \text{(ref. 14)} \quad (1)$$

$$\delta^{13}\mathrm{C} = 175.7 - 0.963\sigma^{13}\mathrm{C}\ \text{(ref. 15)} \quad (2)$$

We have checked that the experimental chemical shifts of 1-(2,4-dinitrophenyl)-2*H*-indazole correspond to rotamer **4′** and not to **4**.

Energies. Concerning the formation of **3** *vs.* **4** (actually **4′**) we have reported in Fig. 1 that the isomer **4** is the most abundant, this being true for the three experimental conditions used: reflux in ethanol, reflux in xylene and fusion without solvent.[1,2] The computed values corresponding to part I of this manuscript are gathered in Table 3 and represented in Fig. 9.

Starting from the most stable tautomer, 1*H*-indazole (**1a**), to reach **4**·HF the barrier has a height of 92.9 kJ mol^{-1} while to reach **3**·HF the barrier is lower, 88.3 kJ mol^{-1}. This is in

Table 2 Experimental chemical shifts (δ, ppm, in DMSO-d_6) and calculated chemical shifts (δ, ppm) of compounds **3** and **4′**

Comp.		H_3	H_4	H_5	H_6	H_7	$H_{3'}$	$H_{4'}$	$H_{5'}$	$H_{6'}$	CHO
^{1}H NMR											
3	Exp.	8.52	7.95	7.38	7.61	7.82	8.92	—	8.65	8.29	—
	Calcd	8.00	7.75	7.31	7.51	7.56	8.71	—	8.50	7.67	—
4′	Exp.	9.08	7.81	7.15	7.35	7.64	8.93	—	8.69	8.29	—
	Calcd	7.74	7.56	7.08	7.26	7.70	8.72	—	8.37	8.34	—

Comp.		C_3	C_{3a}	C_4	C_5	C_6	C_7	C_{7a}	CHO
^{13}C NMR									
3	Exp.	139.0	125.3	122.1	123.2	128.5	110.2	136.1	—
	Calcd	138.7	127.9	122.0	123.0	127.9	108.4	139.2	—
4′	Exp.	128.5	123.2	121.8	122.0	128.8	118.2	150.8	—
	Calcd	122.9	126.0	120.8	124.2	128.9	119.6	152.2	—

		$C_{1'}$	$C_{2'}$	$C_{3'}$	$C_{4'}$	$C_{5'}$	$C_{6'}$
3	Exp.	143.5	138.6	121.7	145.2	128.7	126.2
	Calcd	140.3	147.2	123.7	145.0	126.7	123.1
4′	Exp.	137.3	144.6	122.0	147.2	128.5	128.7
	Calcd	140.0	144.4	122.5	145.5	127.4	128.3

Table 1 Torsion angles (°, absolute values) calculated at the B3LYP/6-311++G(d,p) level

Molecule	Calculated		Experimental
3	N2–N1–C1′–C2′ = 41.0 C1′–C2′–N–O = 46.4 C3′–C4′–N–O = 0.6	N2–N1–C1′–C2′ = 35.5 C1′–C2′–N–O = 53.1 C3′–C4′–N–O = 4.5	
4[a]	N1–N2–C1′–C2′ = 42.2 C1′–C2′–N–O = 48.6 C3′–C4′–N–O = 0.0	N1–N2–C1′–C2′ = 29.1 C1′–C2′–N–O = 63.1 C3′–C4′–N–O = 9.0	N1–N2–C1′–C2′ = 28.0 C1′–C2′–N–O = 66.0 C3′–C4′–N–O = 6.7
4′	N1–N2–C1′–C2′ = 149.8 C1′–C2′–N–O = 47.1 C3′–C4′–N–O = 0.1		

[a] Two independent molecules in the unit cell.

This journal is © The Royal Society of Chemistry and the Centre National de la Recherche Scientifique 2013

Published on 01 May 2013. Downloaded by Fudan University on 31/05/2013 12:55:02.

Table 3 Computed energy values for the formation of 1-(2,4-dinitrophenyl)-1*H*-indazole (**3**) and 2-(2,4-dinitrophenyl)-2*H*-indazole (**4**) corresponding to PCM(EtOH)/B3LYP/6-31G(d)+ZPE calculations (absolute values in hartrees, relative values in kJ mol^{-1})

Entry	Total energy	E_{rel} (with regard to **1a**···**2**)	E_{rel} (with regard to **1b**···**2**)
1a + **2**	−1120.11382	11.7	
1a···**2**	−1120.11834	0.0	
TS1	−1120.08842	78.7	
INT1	−1120.09189	69.5	
TS2	−1120.07854	104.6	
4 + HF	−1120.11488	9.2	
4	−1019.68197		
1b + **2**	−1120.10692	30.1	12.9
1b···**2**	−1120.11182	17.2	0.0
TS3	−1120.08263	93.7	76.5
INT2	−1120.08644	83.7	66.5
TS4	−1120.08025	100.0	82.8
3 + HF	−1120.12156	−8.4	−25.6
3	−1019.69031		

contradiction with the data of Fig. 1 (the most abundant being isomer **4**) but the difference only amounts to 4.6 kJ mol^{-1}. The reaction between **2** and saturated amines has activation barriers in the 65–80 kJ mol^{-1} range,[16] in reasonable agreement with those we have calculated taking into account the differences between indazole and aliphatic amines.

Part II: structure and the mechanism of formation of the 2-(1*N*-oxide-6-nitro-2*H*-benzotriazol-2-yl)benzaldehyde (5)

Crystallography. Crystal packing is formed by double chains parallel to the *ab* plane (Fig. 10). One chain is formed by hydrogen bonds C–H···O between the oxygen atom O(4) of the nitro group N(4) of one molecule, and the hydrogen (H4) of the phenyl carbon (C4) of other molecule along the *ab* plane, and is connected to an antiparallel chain by C–H···O hydrogen bonds between the oxygen atom O(1) of the formyl group of one chain and the hydrogen (H11) of the phenyl carbon (C11) of the other chain, forming a double chain. This interaction fixes the unexpected disposition of the formyl group (Fig. 11–13).

Optimized geometries *vs.* experimental geometries. Neglecting the conformation of the nitro group, compound **5** is characterized by two torsion angles, the first one (θ_1) about the N2–C1′ bond (interring, N1–N2–C1′–C6′) and the second one (θ_2) about the C2′–C(O) bond (formyl group, C3′–C2′–C–O). Thus, four minima are possible if all structures corresponding to two different angles are stable. Actually, one of them is not a minimum (Fig. 14). The three other structures have very similar energies with differences below 2 kJ mol^{-1}, the most stable being **5b** (−1020.16370 hartrees).

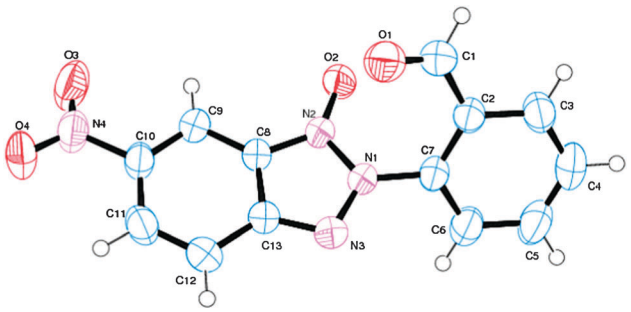

Fig. 10 A view of **5** with displacement ellipsoids drawn at the 50% probability level. The numbering does not follow the systematic one.

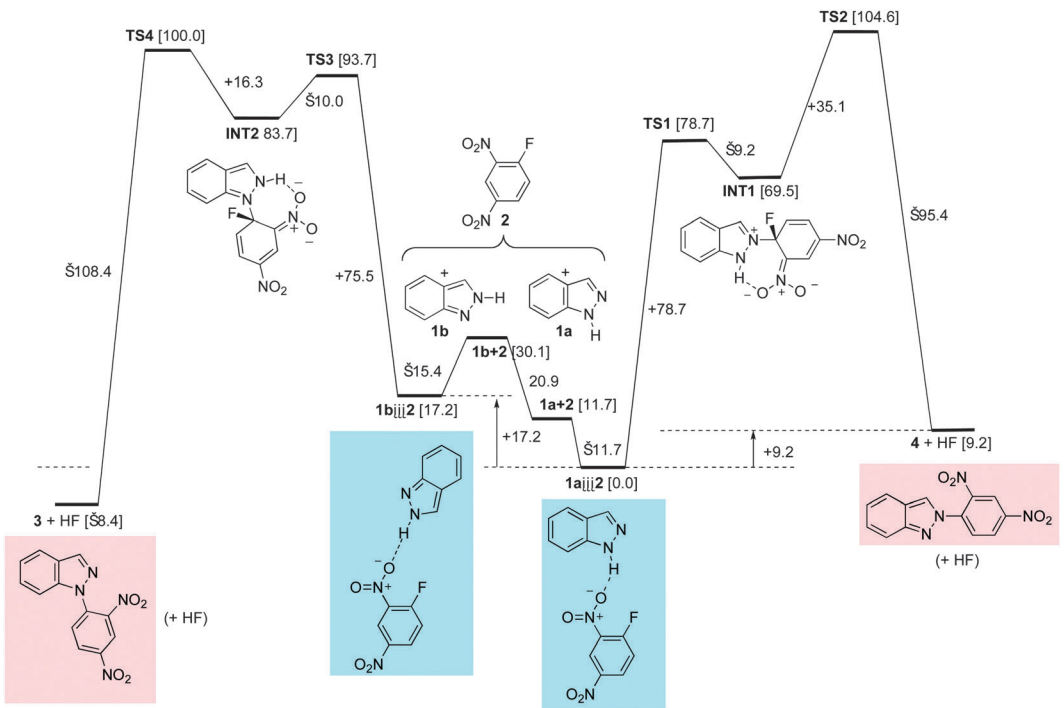

Fig. 9 Energy profile (kJ mol^{-1}) of the formation of **3** and **4** from **1** and **2b** (PCM: ethanol).

Published on 01 May 2013. Downloaded by Fudan University on 31/05/2013 12:55:02.

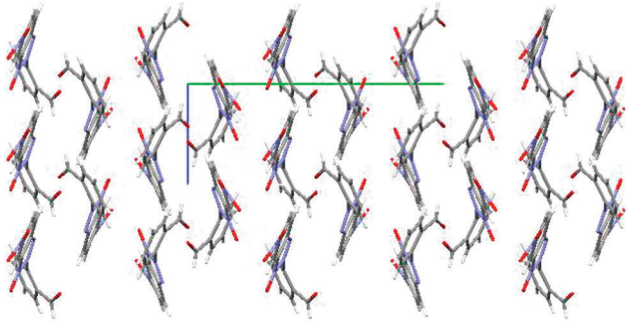

Fig. 11 View of the chains along the *ab* plane of **5**.

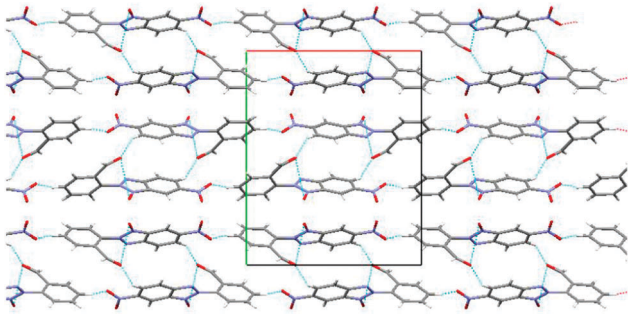

Fig. 12 View of **5** along the *c* axis. Chains parallel to the *ab* plane.

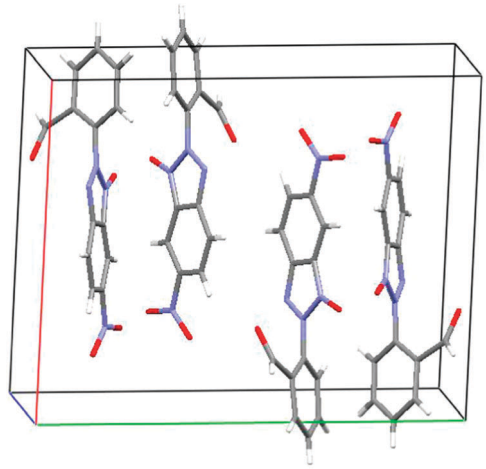

Fig. 13 Packing diagram of **5**.

The experimental X-ray geometry corresponds to **5c**. The stabilization of these structures is of different origin. For **5a** and **5b**, they are due to hydrogen bonds (HBs) but for **5c** there is a single HB, the other stabilizing force is an orthogonal interaction between the O of the carbonyl group and the N2 nitrogen of the benzotriazole *N*-oxide,[13] which bears a partial positive charge (note that the corresponding resonance form is benzenoid while the more common representation is quinonoid). This orthogonal interaction is clearly apparent in the AIM analysis (Fig. 15).

NMR spectroscopy and GIAO/DFT calculations. The chemical shifts, experimental and calculated, for compound **5** are reported in Table 4. The experimental chemical shifts are the geometrical average of two or three conformations if one assumes the simplification of considering only the minima. The test of validity of the multiple regressions is not only the correlation coefficient but, mainly, the fact that the sum of individual populations should be close to 1 (or the percentages close to 100). Imposing the intercept to be 0, the following results are obtained:

From ^{1}H NMR chemical shifts: 23.7% **5a**, 23.6% **5b**, 54.0% **5c** (sum: 101.3%). From ^{13}C NMR chemical shifts: 33.2% **5a**, 23.1% **5b**, 43.8% **5c** (sum: 100.1%).

The results based on ^{13}C chemical shifts should be more reliable (greater range) but, in any case, there are about 25% of each **5a** and **5b** (s*E* isomers) and 50% of **5c** (s*Z* isomer).

If all the values of Tables 2 and 4 are considered together, the ^{1}H chemical shifts (24 values) are well correlated ($R^2 > 0.90$) and the ^{13}C chemical shifts (39 values) still better ($R^2 > 0.98$).

The mechanism of formation of 5. All our attempts to characterize a reaction mechanism compatible with that proposed in 1967–1968 met with no success. Formation of **5** was found to be symmetry forbidden and other possible (3+2) reaction paths led to dead ends. We therefore investigated the reaction mechanism outlined in Fig. 16 by computing the reaction profile. The possible stationary points were located and characterized at the B3LYP/6-31G* level of theory in ethanol solution (*vide infra*). The relative energies of all the stationary points and the shape of the corresponding transition structures are reported in Fig. 17 (all values in kJ mol^{-1}).

Formation of both **4′** (a rotamer of **4**) and **5** starts with the stepwise aromatic nucleophilic substitution reaction of 1*H*-indazole **1** with 1-fluoro-2-nitrobenzene **2**. Despite the partial stabilization of saddle point **TS1** by a weak N–O···H hydrogen bond (see Fig. S1 in the ESI‡), the computed activation energy for the addition step is the largest one along the reaction profile leading to **4**, as it is expected for this kind of reactions. The substitution product **4** is obtained by *syn*-elimination of HF from the unstable addition intermediate **INT1**, recovery of aromaticity of the nitrophenyl moiety being the driving force for this step. It is noteworthy that **4** lies 9.2 kJ mol^{-1} above the complex **1a**···**2** (Fig. 16).

The sequence of stationary points leading to **5** involves the addition of oxygen O*d* of the nitro-nitronate group on the C*e* atom of **1** *via* transition structure **TS5**. As it can be seen by inspection of the geometric features of **TS5**, at this step the N*a*–C*b* bond is already formed, and the whole structure is also partially stabilized by an intramolecular hydrogen bond (see Fig. S1 in the ESI‡). The activation energy associated with this step is also noticeable and corresponds to a stepwise (4+2) cycloaddition between the C*e*═N*a* moiety of **1** and **2**. It is interesting to note that (4+2) cycloaddition (hetero Diels–Alder) chemistry involving nitroalkenes in the presence of Lewis acids has been described by Denmark *et al.*[17] and, more recently and within a different context, by Danishefsky and Houk *et al.*[18]

The (4+2) hetero Diels–Alder cycloadduct **INT3** can eliminate one equivalent of HF to yield the aromatized intermediate **INT4** *via* **TS6** in a similar way to that computed for **INT1** (Fig. 16 and 17).

This journal is © The Royal Society of Chemistry and the Centre National de la Recherche Scientifique 2013

Published on 01 May 2013. Downloaded by Fudan University on 31/05/2013 12:55:02.

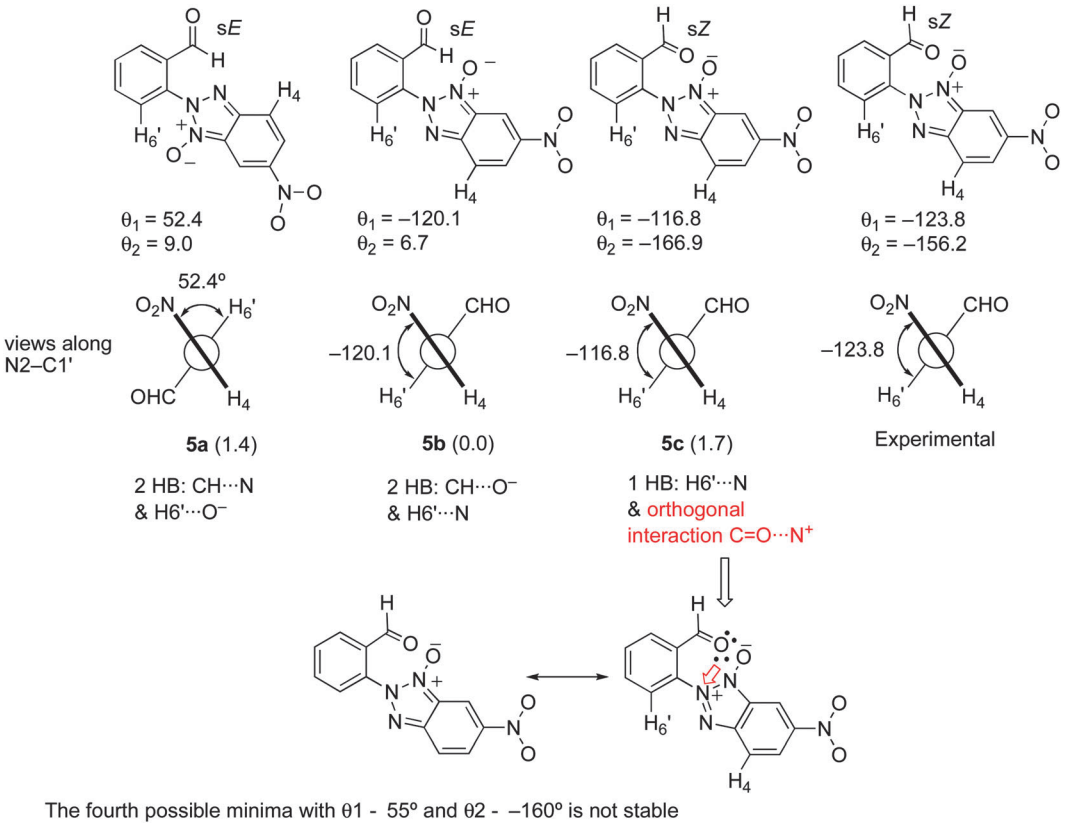

Fig. 14 The calculated and experimental conformations of benzotriazole-*N*-oxide **5** (in parentheses, relative energies).

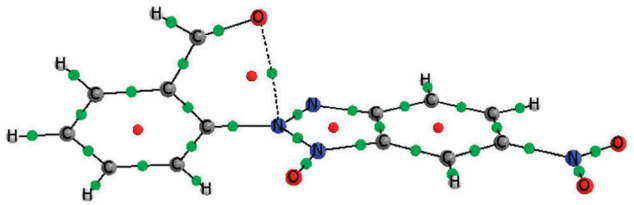

Fig. 15 AIM molecular graphs of compound **5c** optimized at the B3LYP/6-311++G(d,p) computational level. The atoms are labeled O, N, C and H. The bond critical points are pale grey and the ring critical points are dark grey. The following colors will appear in the electronic version: red: oxygen; blue: nitrogen; gray: carbon; white: hydrogen. Bond critical points: green; ring critical points: red.

Unstable zwitterionic species **INT4** yields (*E*)-2-((2-nitroso-phenyl)-diazenyl) benzaldehyde conformers **8** and **8′** *via* concerted cleavage of N*a*–C*e* and O*d*–C*f* bonds. Surprisingly, the activation energy associated with this retro-(4+2) cycloaddition is quite low, the reaction energy leading to benzaldehyde derivative **8** being quite exothermic (Fig. 16). From this latter local minimum, cyclization to **5** takes place smoothly *via* a kinetically favored [5-*exo*-*trig*] process[19] whose associated transition structure is **TS9** (Fig. 15 and 16). Interestingly, the reaction energy (ΔE_{rxn}) associated with the **1a**···**2** → **5** reaction is computed to be −30.0 kJ mol^{-1}, whereas for the **1a**···**2** → **4** transformation it is found that ΔE_{rxn} = +9.2 kJ mol^{-1}. Therefore, thermodynamic control favors formation of **5** as highly polar zwitterionic intermediates are involved in its formation. Although on the basis of our computational results, we dare to predict that microwave irradiation[20] should increase the yield of **5** and its analogues, the calculated barrier to reach **5** from **1a**···**2** is 231.4 kJ mol^{-1}, too high to be involved in the formation of the benzotriazole-*N*-oxide and the mechanism depicted in Fig. 17 must be rejected.

Table 4 Experimental chemical shifts [δ, ppm, ^{1}H (400 MHz) and ^{13}C (100 MHz) in $CDCl_3$] of compound **5** and calculated chemical shifts (δ, ppm) for three minimum conformations of compound **5**

Comp.		H_4	H_5	H_7	$H_{3'}$	$H_{4'}$	$H_{5'}$	$H_{6'}$	CHO
^{1}H NMR									
5	Exp.	7.94	8.31	8.85	8.14	7.90	7.90	7.74	9.93
5a	Calcd	7.68	8.36	8.86	8.44	7.65	7.66	7.91	9.90
5b	Calcd	7.70	8.27	8.84	8.44	7.72	7.69	7.42	9.65
5c	Calcd	7.64	8.25	8.78	7.81	7.83	7.73	7.45	10.05

Comp.		C_{3a}	C_4	C_5	C_6	C_7	C_{7a}	CHO
^{13}C NMR								
5	Exp.	142.6	120.9	128.2	145.7	113.1	124.4	187.5
5a	Calcd	142.6	119.7	124.7	145.6	114.6	125.5	184.1
5b	Calcd	142.8	120.0	124.6	145.6	114.5	124.8	182.7
5c	Calcd	142.7	119.8	123.8	145.2	114.9	125.6	185.3

		$C_{1'}$	$C_{2'}$	$C_{3'}$	$C_{4'}$	$C_{5'}$	$C_{6'}$
5	Exp.	132.6	131.9	131.6	132.5	134.5	123.7
5a	Calcd	137.4	131.1	129.9	131.0	132.8	127.3
5b	Calcd	136.8	131.8	128.8	131.5	133.5	127.3
5c	Calcd	133.6	133.4	135.0	131.3	133.6	129.4

Published on 01 May 2013. Downloaded by Fudan University on 31/05/2013 12:55:02.

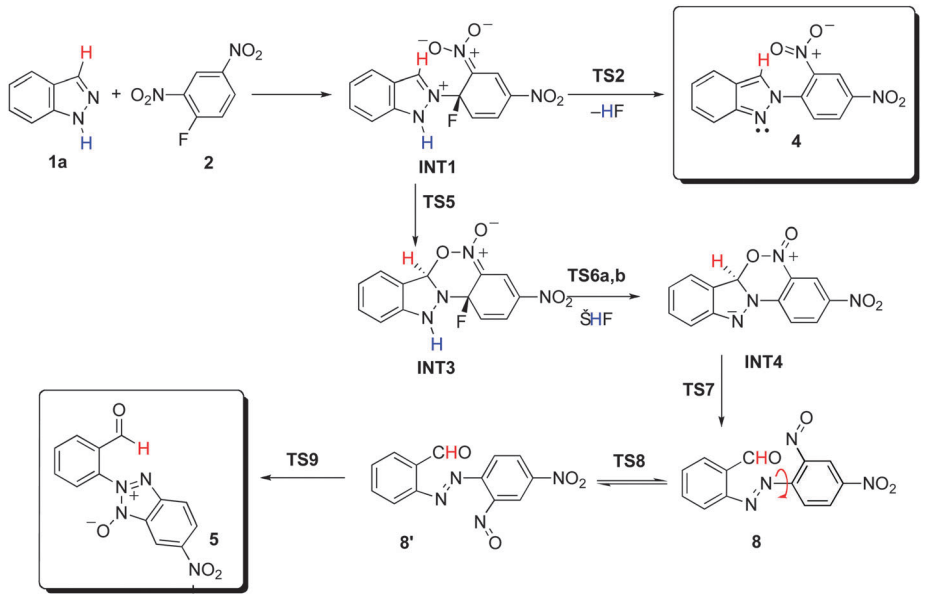

Fig. 16 Mechanism connecting 1*H*-indazole (**1a**) and 1-fluoro-2,4-dinitrobenzene (**2**) to the final products **4** and **5**.

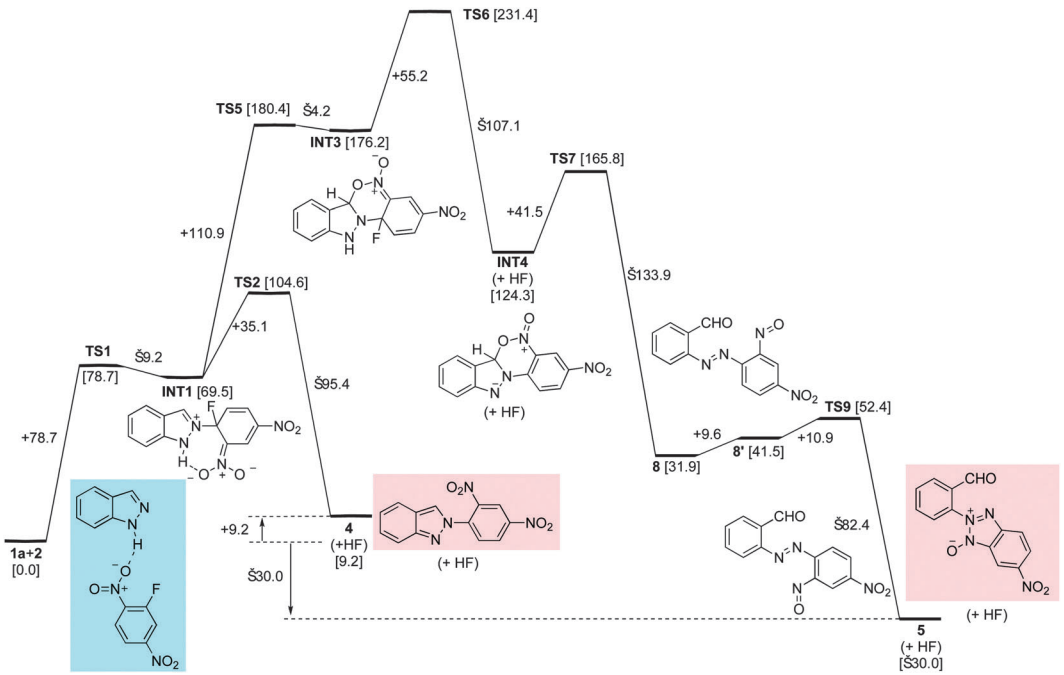

Fig. 17 Reaction profile for the transformation of **1a** and **2** into either **4** or **5**. All the relative energies have been computed in ethanol at the B3LYP(PCM)/6-31G*+ ΔZPVE level and are given in kJ mol^{-1}. The part concerning the formation of **4′** is common with Fig. 9.

We think that **5** could be obtained by thermal isomerization of **4** but all our attempts (see Experimental section) failed; then, since one mole of HF was formed during the reaction (see Fig. 9 and 16), we carried out experiments under conditions as energetic as MW irradiation of a trifluoroacetic solution of **4** containing some drops of H_2SO_4 100%. In all cases, compound **4** was recovered unchanged. The only remaining possibility[21] was that **5** was formed by a photochemical process.

The 1967 reaction[1] was carried out using ordinary glass (not Pyrex) and compound **5** was isolated pure by fractional crystallization in ethanol. We repeated the reaction (10 min reflux in ethanol) using actinic glassware: we obtained 30% of **3** and 70% of **4** (by HPLC) without traces of **5**. The proportions are similar to our previous ones taking into account that the amount of **5** should be added to that of **4**. At 300 K, the 30/70 ratio corresponds to a difference of 2.1 kJ mol^{-1}.

 This journal is © The Royal Society of Chemistry and the Centre National de la Recherche Scientifique 2013

Published on 01 May 2013. Downloaded by Fudan University on 31/05/2013 12:55:02.

Finally, we irradiated a sample of **4** in ethanol and obtained **5** in quantitative yield; the reaction was the same in a degassed solution (Ar bubbled through it) and in solution where oxygen (air) as a quencher[22] had been bubbled, thus proving that the reaction occurs *via* the singlet.[23] The formation of oxygen–carbon bonds upon irradiation has been reported previously but on very different compounds: 1-(2,4-dinitrophenyl) and 1-(2,4,6-trinitrophenyl)aziridines,[24] and 1-aryl-2-nitroalkenes (photochromism).[25]

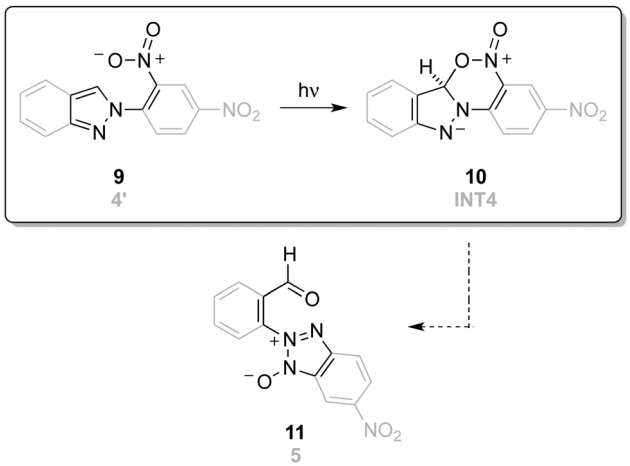

Fig. 18 Model system used to explore the photochemical formation of six-membered intermediate **INT4**. The species included in the experimental studies are indicated in grey.

In order to investigate the photochemical conversion of **4** to **5** on the S_0 and S_1 potential energy hypersurfaces associated with the singlet ground state and the first excited singlet state, respectively, we decided to explore the behavior of a computationally simpler system. The critical step on the S_0 ground state reaction coordinate was the formation of **INT4**, whose combined activation energies from **4** were calculated to be prohibitively high. Since in the photochemical experiments the neutral species **4** was used as starting material, we explored this step using the **9** → **10** transformation as a model system (Fig. 18).

A standard DFT study (Fig. 19A) on the thermal **9** → **10** reaction at the B3LYP/6-31G* level of theory led to the characterization of transition structure $\mathbf{12}_{TS}(S_0)$ on the ground state S_0 hypersurface, with an activation energy of 192 kJ mol^{-1}, in line with the high barriers previously computed for this kind of reaction. Time-dependent DFT (TDDFT) calculations performed with the same hybrid functional and the basis set led to a vertical transition of type nπ*. This electronic transition involves a double excitation from the HOMO − 2 Kohn–Sham

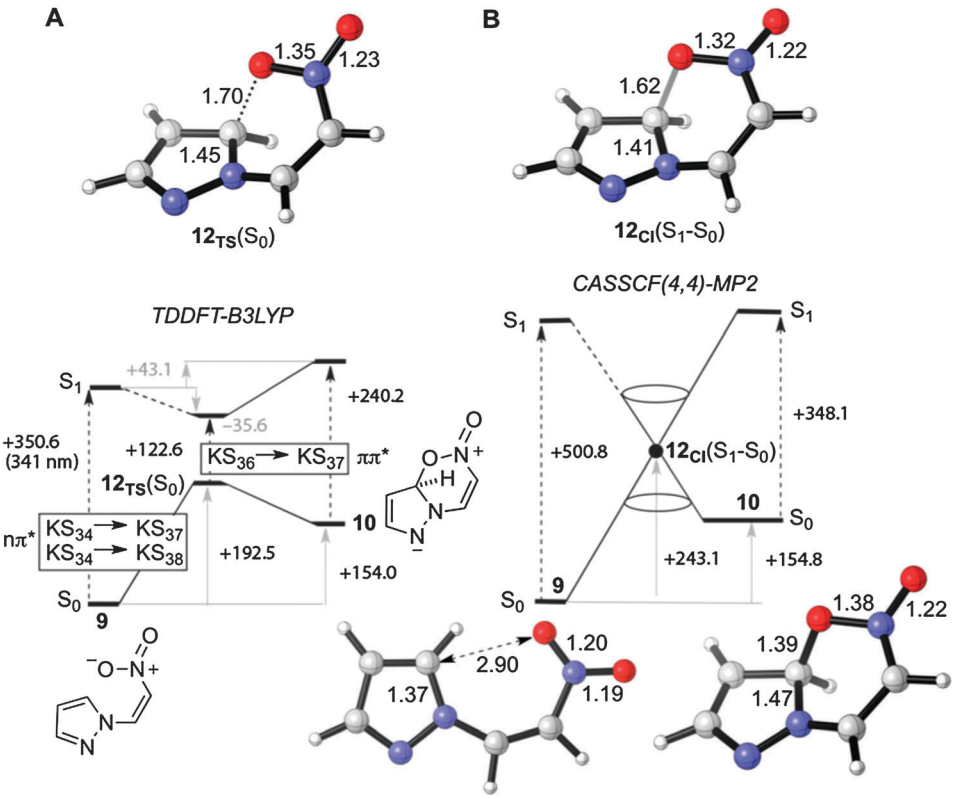

Fig. 19 Computational profiles associated with the **9** → **10** reaction. Bond distances are given in Å. Relative energies are reported in kJ mol^{-1}. Grey arrows connect fully optimized structures. Dashed arrows indicate vertical transitions. (A) B3LYP/6-61G* and time-dependent DFT (TDDFT) B3LYP/6-31G* profiles. KS_i → KS_j indicates the Kohn–Sham (KS) orbitals involved in the corresponding transition. $\mathbf{12}_{TS}(S_0)$ is the transition structure (TS) that connects local minima **9** and **10** in the S_0 ground state. (B) CASSCF(4,4)-MP2/6-31G*//CASSCF(4,4)/6-31G* profile for the same process. $\mathbf{12}_{CI}(S_1–S_0)$ is the conical intersection (CI) that connects **9** on the S_1 hypersurface with **10** in the S_0 ground state.

Published on 01 May 2013. Downloaded by Fudan University on 31/05/2013 12:55:02.

(KS) orbital, mainly formed by lone pairs of the nitro and pyrazole groups, to the LUMO and LUMO + 1, both of them involving delocalized π-systems. Despite its low absorptive capacity, at this point the S_1 state has a vertical excitation energy of 341 nm (equivalent to 350.6 kJ mol^{-1}), a transition therefore quite close to the visible region (380–740 nm), within the accuracy limits of TDDFT.[26] It is expected that in more conjugated systems such as **4** the wavelength associated with this kind of transition lies in the visible region. Interestingly, the S_0–S_1 vertical transition of $\mathbf{12_{TS}}$ was calculated to be of only *ca.* 121 kJ mol^{-1} and is associated with a symmetry allowed ππ* HOMO–LUMO transition (Fig. 19A). As a consequence, $\mathbf{12_{TS}}$ in the S_1 state lies *ca.* 33 kJ mol^{-1} below **9** and *ca.* 84 kJ mol^{-1} below **10**. This situation suggested that there should be a conical intersection (CI) connecting both S_0 and S_1 potential energy hypersurfaces and therefore stationary points **9** and **10**.

We carried out CASSCF(4,4)-MP2/6-31G*//CASSCF(4,4)/6-31G* calculation[27] (Fig. 19B) in order to locate this hypothetical conical intersection. These multiconfigurational SCF (MC-SCF) calculations were performed by checking the Kohn–Sham orbitals involved in the S_0–S_1 transitions and the corresponding canonical MOs. According to the TDDFT results, the starting guess was modified in order to include MO_{34} (which is similar to KS_{34}) in the active space of **9**. In the case of **12** and **10**, the simpler HOMO–LUMO transition found in the TDDFT calculations resulted in rapidly convergent CASSCF solutions. Actually, for these latter stationary points the CASSCF(2,2) and CASSCF(4,4) results were very similar. Under these conditions we readily located conical intersection $\mathbf{12_{CI}}$ at the CASSCF(4,4)/6-31G* level by starting the optimization from the B3LYP/6-31G* geometry and wave function of $\mathbf{12_{TS}}$ (Fig. 19A). As expected, the chief geometric features of $\mathbf{12_{CI}}$ were found to be very similar to those computed for $\mathbf{12_{TS}}$, the critical C–O bond distance being a little bit shorter, thus indicating a more advanced structure towards intermediate **10**.

From these TDDFT and MC-SCF computational results, we conclude that the reactions indicated in Fig. 17 can be readily performed under UV-visible irradiation. The photochemical reaction path starts with a relatively low energy S_0–S_1 excitation. From this nπ* S_1 excited state the system evolves to a ππ* state and relaxes to the S_0 state *via* a conical intersection very similar to the transition structure that connects reactants and products under purely thermal conditions. Beyond this latter stationary point, the rest of the elementary steps leading to **5** can occur on the S_0 potential energy hypersurface.

Conclusions

The most significant conclusions obtained from the results reported in this paper are:

– The X-ray structures of **3** and **4** have been determined both having the nitro group near the N atom of the indazole ring. The structure of **5** presents an interesting example of orthogonal interaction.

– ^{1}H and specially ^{13}C NMR chemical shifts show that in DMSO 1-(2,4-dinitrophenyl)-2*H*-indazole has the nitro group near the N atom (**3**) while 2-(2,4-dinitrophenyl)-2*H*-indazole has the nitro group near the CH (conformation **4′**).

– The mechanism of formation of both *N*-substituted indazoles is a classical one and the calculated transition states have reasonable values.

– The only found thermal mechanism of formation of 2-(1*N*-oxide-6-nitro-2*H*-benzotriazol-2-yl)benzaldehyde differs considerably from that proposed in 1967–1968. It involves five TSs and five intermediates that have been theoretically characterized. However, it is too high in energy (231 kJ mol^{-1}) to be operative.

– The **4** to **5** transformation is a photoisomerization going through the singlet state. This is the first reported example of such a reaction.

– A mechanism has been theoretically calculated for the singlet state photoisomerization.

Experimental section

Chemistry

General methods. All reagents were purchased from commercial suppliers and used without further purification. Flash chromatography was performed on silica gel (230–400 mesh). Melting points are uncorrected. Microwave reactions were carried out using a Biotage Initiator™ 2,0. Most ^{1}H and ^{13}C NMR spectra were obtained at 300 MHz (^{1}H; ^{13}C 75 MHz) at 298 K and one at 400 MHz for the ^{1}H NMR spectrum of **5**. Abbreviations for multiplicity are as follows: d indicates doublet, t indicates triplet, m indicates multiplet, bs indicates broad singlet, bd indicates broad doublet, dd indicates double doublet, dt indicates double triplet. Chemical shifts are reported in ppm referenced to TMS for $CDCl_3$ and to the internal solvent residual of DMSO-d_6 at 2.50 ppm for ^{1}H NMR and at 39.5 ppm for ^{13}C NMR. Assignment of the ^{1}H and ^{13}C NMR signals was based on the ^{1}H–^{1}H spin–spin coupling constants as well as on COSY, HMBC and HSQC methods. LC-MS analyses were performed using an Alliance 2695 (Waters) with a diode array UV/Vis detector Waters 2996 and interfaced to a Micromass ZQ mass spectrometer; analyses were performed using reversed phase HPLC silica based columns: column bridge C18 3.5 μm. (2.1 × 100 mm). Using an injection volume of 3 μL, a flow rate of 0.25 mL min^{-1} and gradient elution (5 to 95% over 5 min) of acetonitrile in water. Acetonitrile contains 0.08% v/v and water contains 0.1% v/v formic acid. Analyses were monitored at 254 nm wavelength.

The photoreactions were performed in quartz cells. The solutions were irradiated through a dichroic mirror (Dichroic Beam Turning Mirror, Oriel) to cut off UV light (transmission range 260–320 nm) by using a mercury (Xe) lamp (Oriel Research Arc Lamp Source, 400 W). A focusing lens (Fiber Bundle Focusing Assembly, Fused Silica Aspheric, F/2.2, 4 mm Typical Spot Size) was also used. The irradiation was controlled using an electronic shutter (Electronic Shutter Driver, Oriel), a light intensity controller and a digital timer (Oriel, RS-232).

Purification of the three compounds previously obtained[1]. Using a flash chromatography column (eluent 5 : 1 dichloromethane–hexane → 9 : 1 dichloromethane–methanol), four fractions were isolated: **3**

 This journal is © The Royal Society of Chemistry and the Centre National de la Recherche Scientifique 2013

Published on 01 May 2013. Downloaded by Fudan University on 31/05/2013 12:55:02.

was obtained pure in the first fraction, **4** was recrystallized from ethanol from the second fraction, and **5** was recrystallized from acetonitrile from the third fraction. Fourth fraction was a mixture of **5** and an unknown compound, which was identified as the hemiacetal of **5** formed by reaction with traces of ethanol (see ESI‡).

1-(2,4-Dinitrophenyl)-1*H*-indazole (**3**): yellow crystals. M_p = 172–173 °C. Lit. m.p. 172 °C.[1] ^{1}H-NMR (300 MHz, DMSO-d_6) δ ppm: 8.92 ($H_{3'}$ Ar, d, J = 2.5 Hz, 1H), 8.65 ($H_{5'}$ Ar, dd, J = 8.9 Hz, J = 2.5 Hz, 1H), 8.52 (H_3 indazole, bd, J = 0.9 Hz, 1H), 8.29 ($H_{6'}$ Ar, d, J = 8.9 Hz, 1H), 7.95 (H_4 indazole, dd, J = 8.1 Hz, J = 0.9 Hz, 1H), 7.82 (H_7 indazole, d, J = 8.1 Hz, 1H), 7.61 (H_6 indazole, dt, J = 8.1 Hz, J = 0.9 Hz, 1H), 7.38 (H_5 indazole, dt, J = 8.1 Hz, J = 0.9 Hz, 1H). ^{13}C-NMR (75 MHz, DMSO-d_6) δ ppm: 145.2 $C_{4'}$, 143.5 $C_{1'}$, 139.0 C_3, 138.6 $C_{2'}$, 136.1 C_{7a}, 128.7 $C_{5'}$, 128.5 C_6, 126.2 $C_{6'}$, 125.3 C_{3a}, 123.2 C_5, 122.1 C_4, 121.7 $C_{3'}$, 110.2 C_7. LC/MS: positive ESI-MS: m/z = 285.20 $[M + H]^+$ (100%); HPLC: t_R = 5.06 min (99%); eluent: gradient from 10% MeCN + 0.08% formic acid and 90% H_2O + 0.1% formic acid to 100% MeCN + 0.08% formic acid; flow = 1 mL min^{-1}; λ = 256 nm. Proper crystals of **3** for X-ray diffraction were obtained by recrystallization from EtOH with some drops of hexane.

2-(2,4-Dinitrophenyl)-2*H*-indazole (**4**): yellow solid. M_p = 152–154 °C. Lit. m.p. 158 °C.[1] ^{1}H-NMR (400 MHz, DMSO-d_6) δ ppm: 9.08 (H_3 indazole, bs, 1H), 8.93 ($H_{3'}$ Ar, d, J = 2.4 Hz, 1H), 8.69 ($H_{5'}$ Ar, dd, J = 8.7 Hz, J = 2.4 Hz, 1H), 8.29 ($H_{6'}$ Ar, d, J = 8.7 Hz, 1H), 7.81 (H_4 indazole, d, J = 8.6 Hz, 1H), 7.64 (H_7 indazole, d, J = 8.6 Hz, 1H), 7.35 (H_6 indazole, t, J = 7.2 Hz, 1H), 7.15 (H_5 indazole, t, J = 7.2 Hz, 1H). ^{13}C-NMR (75 MHz, DMSO-d_6) δ ppm: 150.8 C_{7a}, 147.2 $C_{4'}$, 144.6 $C_{2'}$, 137.3 $C_{1'}$, 128.8. C_6, 128.7 $C_{6'}$, 128.5 C_3, $C_{5'}$, 126.2 $C_{6'}$, 123.7 $C_{3'}$, 123.2 C_{3a}, 122.0 C_5, 121.8 C_4, 118.2 C_7. LC/MS: positive ESI-MS: m/z = 285.20 $[M + H]^+$ (100%); HPLC: t_R = 4.90 min (90%); eluent: gradient from 10% MeCN + 0.08% formic acid and 90% H_2O + 0.1% formic acid to 100% MeCN + 0.08% formic acid; flow = 1 mL min^{-1}; λ = 256 nm. Proper crystals of **4** for X-ray diffraction were obtained by recrystallization from dichloromethane with some drops of hexane.

2-(1*N*-Oxide-6-nitro-2*H*-benzotriazol-2-yl)-benzaldehyde (**5**): light yellow powder. M_p = 212–214 °C. Lit. m.p. 206 °C.[1] ^{1}H-NMR (400 MHz, $CDCl_3$) δ ppm: 9.93 (CHO, s, 1H); 8.85 (H_7, d, J = 2.0, 1H), 8.31 (H_5, q, J = 9.4, J = 2.0 Hz, 1H), 8.14 ($H_{3'}$, q, J = 6.6, J = 2.3, 1H), 7.94 (H_4, d, J = 9.4 Hz, 1H), 7.9 ($H_{4'}$ and $H_{5'}$, septuplet), 7.74 ($H_{6'}$, q, J = 7.0, J = 2.0 Hz, 1H). ^{13}C-NMR (75 MHz, DMSO-d_6) δ ppm: 190.2 CHO, 145.2 C_6, 142.0 C_{3a}, 135.0 $C_{5'}$, 132.7 $C_{4'}$, 132.4 $C_{1'}$, 131.2 $C_{2'}$, 123.4 $C_{6'}$, 128.7 C_5, 124.1 C_{7a}, 123.4 $C_{6'}$, 131.0 $C_{3'}$, 121.1 C_4, 112.6 C_7. LC/MS: positive ESI-MS: m/z = 284.94 $[M + H]^+$ (100%); HPLC: t_R = 4.28 min (99%); eluent: gradient from 10% MeCN + 0.08% formic acid and 90% H_2O + 0.1% formic acid to 100% MeCN + 0.08% formic acid; flow = 1 mL min^{-1}; λ = 256 nm. Proper crystals of **5** for X-ray diffraction were obtained by recrystallization from EtOH–water 5 : 1 with some drops of hexane.

*Thermal isomerization experiments of 2-(2,4-dinitrophenyl)-2H-indazole (**4**).* Neutral conditions: a solution of 2-(2,4-dinitrophenyl)-2*H*-indazole (6 mg, 0.02 mmol) in xylene (10 mL) was refluxed for 22 h. The solvent was evaporated at reduced pressure yielding a light yellow solid. LC-MS retention time 4.88 min $[M + H]^+$ = 285. Acid conditions: to a solution of 2-(2,4-dinitrophenyl)-2*H*-indazole (6 mg, 0.02 mmol) in trifluoroacetic acid (10 mL) two drops of H_2SO_4 100% were added. The reaction mixture was refluxed for 22 h. The solvent was evaporated at reduced pressure yielding light yellow solid. LC-MS retention time 4.86 min $[M + H]^+$ = 285; 2-(2,4-dinitrophenyl)-2*H*-indazole (6 mg, 0.02 mmol), H_2SO_4 100% (two drops) in TFA (10 mL) were heated at 100 °C for 7 h in a microwave reactor. The mixture was evaporated at reduced pressure yielding a light yellow solid. LC-MS retention time 4.84 min $[M + H]^+$ = 285. Compound **5** has a LC-MS retention time of 4.12 min $[M + H]^+$ = 285.

*Preparation of compounds **3** and **4**.* A solution of indazole (500 mg, 4.2 mmol, 1 equiv.) and 1-fluoro-2,4-dinitrobenzene (530 μL, 4.2 mmol, 1 equiv.) in EtOH (15 mL) was heated at reflux for 19 h in an actinic amber round-bottom flask protected from light. Afterwards, the yellow solid formed was filtered and washed with cold EtOH several times. Solvent was removed from the liquid layer, obtaining an oily brown residue. The solid and the oily residue were dried under vacuum. Solid (832 mg, 69% yield) was identified by TLC and LC/MS as a mixture (68 : 32) of 2-(2,4-dinitrophenyl)-2*H*-indazole and 1-(2,4-dinitrophenyl)-1*H*-indazole, respectively. In the oily residue were found unreacted indazole and two subproducts 2,4-dinitro-1-ethoxybenzene and an unknown one. No traces of **5** were found (^{1}H NMR and LC/MS).

*Photoisomerization of 2-(2,4-dinitrophenyl)-2H-*indazole (**4**). A solution of 2-(2,4-dinitrophenyl)-2*H*-indazole (10^{-4} M) in EtOH was placed in a quartz cell and bubbled with Ar for 40 min before irradiation. Then, the solution was irradiated from 260 to 320 nm for 2 h using a mercury (Xe) lamp (400 W). An analogous experiment was performed by the irradiation of the solution, this time, in the presence of air. The reactions were monitored by HPLC-MS.

Crystallographic study. The structures display no noticeable modifications in crystal packing at different temperatures. Compounds **3** and **4** are formed by chains parallel to the *bc* plane while compound **5** is formed by chains parallel to the *ab* plane. Molecules forming the layers are linked by H-bonds. There are weak intramolecular interactions. For compound **4**, the structure at room temperature does not present changes with that derived from low temperature data, except for the higher structure expansion due to the higher atomic displacements.

Details of crystal structure determinations including crystal data, data collection, structure determination and refinement parameters are shown in Table 5. X-ray diffraction measurements were performed at room temperature for **4** (298.0 K) and **5** (293 K) and at low temperature (120 K) for compounds **3** and **4**, with mirror-monochromated CuKα radiation (λ = 1.5418 Å). Images were collected at 55 mm fixed crystal-detector distance, using the oscillation method with variable exposure time per image. The structures were solved using direct methods and subsequent Fourier differences using in all cases the WingX

Published on 01 May 2013. Downloaded by Fudan University on 31/05/2013 12:55:02.

Table 5 Crystal data and structure refinement for compounds **3**, **4** and **5**

Compound	**3** (120.0 K)	**4** (120.0 K)	**4** (298.0 K)	**5** (293.0 K)
Formula	$C_{13}H_8N_4O_4$	$C_{13}H_8N_4O_4$	$C_{13}H_8N_4O_4$	$C_{13}H_8N_4O_4$
Formula weight/g mol^{-1}	284.23	284.23	284.23	284.23
Wavelength	CuKα (1.5418 Å)	CuKα (1.5418 Å)	CuKα (1.5418 Å)	CuKα (1.5418 Å)
Crystal system	Orthorhombic	Monoclinic	Monoclinic	Monoclinic
Space group	$P2_12_12_1$	$P2_1/c$	$P2_1/c$	$P2_1/c$
a (Å)	7.0459(2)	7.0730(5)	7.2107(6)	13.0325(6)
b (Å)	11.0462(3)	24.0840(16)	24.0635(17)	15.3958(15)
c (Å)	15.4551(4)	14.3289(10)	14.4077(11)	6.1563(3)
α (°)	90.00	90.00	90.00	90
β (°)	90.00	100.633(7)	100.334(17)	99.558(5)
γ (°)	90.00	90.00	90.00	90
Cell volume/Å^3	1203.1(2)	2399.0(3)	2459.4(3)	1218.09(14)
Z	4	8	8	4
Calc. density/mg m^{-3}	1.569	1.574	1.535	1.550
Absorption coefficient/mm^{-1}	1.025	1.028	1.003	1.012
F(000)	584.0	1168.0	1168.0	584.0
Crystal size (mm^3)	0.14 × 0.08 × 0.06	0.25 × 0.05 × 0.01	0.28 × 0.02 × 0.01	0.20 × 0.10 × 0.03
Index ranges	$-8 \le h \le 8$, $-11 \le k \le 13$, $-15 \le l \le 18$	$-7 \le h \le 8$, $-29 \le k \le 28$, $-15 \le l \le 17$	$-8 \le h \le 7$, $-23 \le k \le 29$, $-17 \le l \le 12$	$-15 \le h \le 14$, $-18 \le k \le 18$, $-7 \le l \le 7$
2Θ range for data collection (°)	9.84 to 140.82	7.28 to 141.34°	7.24 to 141.42	6.88 to 141.62
Reflections collected	4652	16197	8843	13 222
Independent reflections	2258 [R_{int} = 0.0311]	4554 [R_{int} = 0.0795]	4556 [R_{int} = 0.0663]	2317 [R_{int} = 0.0506]
Completeness	0.998 (θ = 68.00°)	1.000 (θ = 68.00°)	0.986 (θ = 68.00°)	0.989 (θ = 70.81°)
Absorption correction	Analytical	Analytical	Analytical	Empirical
Max. and min. transmission	1.00000 and 0.98138	0.987 and 0.873	1.0957 and 0.6170	1.00000 and 0.90640
Refinement method	Full-matrix least-squares on F^2	Full-matrix least-squares on F^2	Full-matrix least-squares on F^2	Full-matrix least-squares on F^2
Data/restraints/parameters	2258/0/190	4554/0/379	4556/0/379	2317/0/190
Goodness-of-fit on F^2	1.073	0.984	0.998	1.048
Final R indices [$I > 2\sigma(I)$]	R_1 = 0.0335, wR_2 = 0.0768	R_1 = 0.0469, wR_2 = 0.0934	R_1 = 0.0599, wR_2 = 0.1241	R_1 = 0.0439, wR_2 = 0.1028
R indices (all data)	R_1 = 0.0383, wR_2 = 0.0796	R_1 = 0.0822, wR_2 = 0.1085	R_1 = 0.1325, wR_2 = 0.1709	R_1 = 0.0676, wR_2 = 0.1171
Largest diff. peak and hole	0.14 and −0.22 e Å^{-3}	0.21 and −0.20 e Å^{-3}	0.19 and −0.29 e Å^{-3}	0.19 and −0.25 e Å^{-3}
Flack parameter	0.3(2)			

package and refined by full-matrix least-squares on F^2. Empirical absorption correction was applied using the program XABS2. All non-H atoms were anisotropically refined. Hydrogen atoms attached to carbon atoms were positioned geometrically with U_{iso} values derived from U_{eq} values of the corresponding carbon atom.

Crystallographic calculations were carried out using the following programs: CrysAlis CCD and RED[28] for data collection, cell refinement, data reduction and empirical absorption correction; SIR 2004[29] for structure solution; SHELXL-97[30] for structure refinement and preparation of materials for publication; PLATON[31] for the geometrical calculations; ORTEP[32] and Mercury[33] for molecular graphics. Crystal data and structure refinement details for the three structures are given in Table 5. Selected bond lengths (Å) and bond angles (°), and hydrogen bonds are listed in Table 6 and 7 for both compounds.

CCDC 806879, 806880, 806881 and 923952, respectively.‡

All the calculations reported in this paper have been performed within Density Functional Theory,[34] using the hybrid three-parameter functional customarily denoted B3LYP.[35] The standard 6-31G(d) basis sets[36] as implemented in the *GAUSSIAN 09*[37] suite of programs have been used in all cases. Solvent effects were taken into account by optimizing geometries and computing energies using the PCM method with ethanol parameters.[38] All stationary points were characterized by harmonic analysis.[39] All transition structures exhibited one and only one imaginary frequency associated with nuclear motion along the reaction coordinate under study. For calculation of absolute shieldings, the B3LYP/6-31G(d) optimized geometries were further optimized at the B3LYP/6-311++G(d,p) level.[40] Absolute shieldings were calculated within the GIAO approximation.[41]

The reactivity of the model systems in the excited state has been carried out using the time-dependent DFT (TDDFT) B3LYP/6-31G(d), CASSCF(4,4)/6-31G(d) and CASSCF(4,4)-MP2/6-31G(d)//CASSCF(4,4)/6-31G(d) computational models within the *GAUSSIAN 09* program.

The bonding characteristics were analyzed by means of the atoms in molecules (AIM) theory.[42,43] For this purpose we have

 This journal is © The Royal Society of Chemistry and the Centre National de la Recherche Scientifique 2013

Published on 01 May 2013. Downloaded by Fudan University on 31/05/2013 12:55:02.

Table 6 Selected bond lengths (Å) and bond angles (°) for **3**, **4** and **5**

Bond lengths (Å)		Bond angles (°)	
3			
O3–N4	1.224(2)	N2–N1–C7	111.2(1)
O1–N3	1.222(2)	N2–N1–C8	118.7(2)
O4–N4	1.225(2)	O1–N3–O2	124.6(2)
N2–N1	1.381(2)	C1–N2–N1	105.5(2)
N1–C7	1.386(2)	O3–N4–O4	124.1(2)
N1–C8	1.395(2)	C10–C11–N4	118.3(2)
N3–C9	1.472(2)	C12–C11–N4	119.3(2)
N2–C1	1.310(3)	N1–C8–C13	120.3(2)
N4–C11	1.465(2)	N1–C8–C9	121.8(2)
		C10–C9–N3	115.8(2)
		C8–C9–N3	121.7(2)
4 298 K			
O2A–N3A	1.219(4)	C1B–N1B–N2B	103.4(3)
O2B–N3B	1.221(5)	C7A–N2A–N1A	113.5(3)
O3A–N4A	1.212(5)	N1A–N2A–C8A	119.2(3)
O4B–N4B	1.229(5)	C1A–N1A–N2A	103.4(3)
O3B–N4B	1.212(5)	O1B–N3B–O2B	125.2(3)
O1A–N3A	1.216(4)	C7B–N2B–N1B	113.2(3)
O1B–N3B	1.211(4)	O3B–N4B–O4B	123.8(4)
N1B–C1B	1.341(5)	O3A–N4A–O4A	123.7(4)
N1B–N2B	1.373(4)	O1A–N3A–O2A	125.5(4)
N2A–C7A	1.356(5)		
N2A–N1A	1.367(4)		
N2A–C8A	1.409(5)		
O4A–N4A	1.220(5)		
N1A–C1A	1.351(5)		
N3B–C13B	1.469(5)		
N2B–C7B	1.349(5)		
N2B–C8B	1.410(5)		
N4B–C11B	1.470(6)		
N4A–O3A	1.212(5)		
N4A–C11A	1.459(6)		
N3A–C13A	1.482(5)		
4 120 K			
O2A–N3A	1.230(3)	C1B–N1B–N2B	103.0(2)
O3A–N4A	1.222(3)	C7A–N2A–N1A	114.0(2)
O4B–N4B	1.227(3)	N1A–N2A–C8A	119.4(2)
O3B–N4B	1.225(3)	C1A–N1A–N2A	103.2(2)
O1A–N3A	1.214(3)	O1B–N3B–O2B	126.0(2)
O1B–N3B	1.218(3)	C7B–N2B–N1B	114.0(2)
N1B–C1B	1.347(3)	O3B–N4B–O4B	124.0(2)
N1B–N2B	1.370(3)	O3A–N4A–O4A	124.5(2)
N2A–C7A	1.362(3)	O1A–N3A–O2A	125.2(2)
N2A–N1A	1.369(3)		
N2A–C8A	1.409(3)		
O4A–N4A	1.228(3)		
N1A–C1A	1.350(3)		
N3B–C13B	1.477(3)		
N2B–C7B	1.353(3)		
N2B–C8B	1.416(3)		
N4B–C11B	1.461(3)		
N4A–C11A	1.468(3)		
N3A–C13A	1.482(3)		
5			
N4–O3	1.217(3)	O3–N4–O4	123.7(2)
N4–O4	1.227(3)	O3–N4–C10	118.6(2)
N4–C10	1.469(3)	O4–N4–C10	117.7(2)
N2–N1	1.361(2)	C8–N2–N1	104.9(1)
N2–C8	1.360(2)	O2–N2–N1	123.7(1)
N2–O2	1.262(2)	O2–N2–C8	131.4(1)
N1–C7	1.421(2)	N2–N1–C7	122.4(1)
N1–N3	1.339(2)	N3–N1–N2	114.1(1)
C2–C1	1.474(3)	N3–N1–C7	123.4(1)
O1–C1	1.202(3)	O1–C1–C2	125.8(2)

Table 7 Hydrogen bonds for compounds **3**, **4** and **5**

D–H···A (Å)	d(D–H)/Å	d(H···A)/Å	d(D···A)/Å	(D–H···A)/°
3				
C6–H6···O4[a]	0.95	2.53	3.237(3)	131
C12–H12···O3[a]	0.95	2.51	3.262(3)	137
C13–H13···O4[a]	0.95	2.52	3.328(3)	142
4 (120 K)				
C2B–H2B···O4B[b]	0.95	2.46	3.2663(5)	143
C7B–H7B···O2B[c]	0.95	2.48	3.394(3)	161
C9B–H9B···O1A[d]	0.95	2.46	3.213(3)	135
C9B–H9B···O2B[c]	0.95	2.51	3.283(3)	139
4 (298 K)				
C2B–H2B···O4B[b]	0.93	2.52	3.319(6)	145
C7B–H7B···O2B[c]	0.93	2.55	3.440(5)	161
C9B–H9B···O1A[d]	0.93	2.50	3.231(6)	136
C9B–H9B···O2B[c]	0.93	2.56	3.319(6)	139
5				
C(4)–H(4)···O(4)[e]	0.93	2.57	3.251(3)	131
C(11)–H(11)···O(1)[f]	0.93	2.57	3.396(3)	148

Symmetry codes:[a] $1-x, -1/2+y, -1/2-z$. [b] $x, 1/2-y, -1/2+z$. [c] $x, 1/2-y, 1/2+z$. [d] x, y, z. [e] $1+x, y, 1+z$. [f] $1-x, -y, -z$.

located the most relevant bond critical points (BCP), and evaluated the electron density at each of them, with the facilities of AIMAll programs.[44] All the interactions were characterized by the presence of a BCP between the atoms involved that are connected by the corresponding bond paths.

Acknowledgements

This work was supported by the Spanish Ministerio de Economía y Competitividad (MAT2010-15094, Factoria de Cristalizacion – Consolider Ingenio 2010) and FEDER funding. We also thank the Ministerio de Ciencia e Innovación (Project No. CTQ 2009-13129-C02-02) and the Comunidad Autónoma de Madrid (Project MADRISOLAR2, ref. S2009/PPQ-1533) for continuing support. Thanks are given to the CTI (CSIC) for an allocation of computer time. F. P. C. thanks the Spanish MICINN (Grants CTQ2010-16959 and Ingenio-Consolider CSD2007-00006) and the Basque Government (GV-EJ, Grant IT-324-07) for financial support. Technical and human support provided by SGIker (UPV/EHU, MICINN, GV/EJ, ESF) is gratefully acknowledged. For the kinetic data discussion and the photochemical experiments and advice we warmly thank Drs José Ignacio García (Universidad de Zaragoza), Ulises Acuña (Instituto de Química-Física ''Rocasolano'', CSIC), Fernando Catalina and Leví López Vilanova (Instituto de Ciencia y Tecnología de Polímeros, CSIC).

Notes and references

1 J. Elguero, A. Fruchier and R. Jacquier, *Bull. Soc. Chim. Fr.*, 1967, 2619.
2 J. Elguero, A. Fruchier and R. Jacquier, *Bull. Soc. Chim. Fr.*, 1968, 3331.
3 J. Elguero, C. Marzin, A. R. Katritzky and P. Linda, *The Tautomerism of Heterocycles*, *Advances in Heterocyclic*

Published on 01 May 2013. Downloaded by Fudan University on 31/05/2013 12:55:02.

Chemistry, Supplement 1, Academic Press, New York, 1976, and references therein.
4 J. Catalán, J. L. G. de Paz and J. Elguero, *J. Chem. Soc., Perkin Trans. 2*, 1996, 57.
5 I. Alkorta and J. Elguero, *J. Phys. Org. Chem.*, 2005, **18**, 719.
6 C. H. Gustafsson, *Finska Kemistamfundets Medd.*, 1938, **1**, 2.
7 J. Sandström, *Acta Chem. Scand.*, 1964, **18**, 871.
8 J. L. M. Abboud, P. Cabildo, T. Cañada, J. Catalán, R. M. Claramunt, J. L. G. de Paz, J. Elguero, H. Homan, R. Notario, C. Toiron and G. I. Yranzo, *J. Org. Chem.*, 1992, **57**, 3938.
9 I. Alkorta and J. Elguero, *J. Org. Chem.*, 2002, **67**, 1515.
10 M. A. García, P. Cabildo, R. M. Claramunt, E. Pinilla, M. R. Torres, I. Alkorta and J. Elguero, *Inorg. Chim. Acta*, 2010, **363**, 1332.
11 W. Baik, T. H. Park, B. H. Kim and Y. M. Jun, *J. Org. Chem.*, 1995, **60**, 5683.
12 B. H. Kim, D. H. Kim, H. J. Park, R. Han, Y. M. Jun and W. Baik, *Bull. Korean Chem. Soc.*, 2001, **22**, 1163.
13 (*a*) R. Paulini, K. Müller and F. Diederich, *Angew. Chem., Int. Ed.*, 2005, **44**, 1788; (*b*) G. P. A. Yap, F. A. Jové, R. M. Claramunt, D. Sanz, I. Alkorta and J. Elguero, *Aust. J. Chem.*, 2005, **58**, 817; (*c*) E. Pinilla, M. R. Torres, R. M. Claramunt, D. Sanz, R. Prakash, S. P. Singh, I. Alkorta and J. Elguero, *ARKIVOC*, 2006, **ii**, 136; (*d*) M. D. S. María, R. M. Claramunt, M. Á. García and J. Elguero, *Tetrahedron*, 2007, **63**, 3737; (*e*) F. R. Fischer, P. A. Wood, F. H. Allen and F. Diederich, *Proc. Natl. Acad. Sci. U. S. A.*, 2008, **195**, 17290; (*f*) N. Triballeau, E. Van Name, G. Laslier, D. Cai, G. Paillard, P. W. Sorensen, R. Hoffmann, H.-O. Bertrand, J. Ngai and F. C. Acher, *Neuron*, 2008, **60**, 767; (*g*) M. Solimannejad, I. Alkorta and J. Elguero, *Chem. Phys. Lett.*, 2009, **474**, 253.
14 A. M. S. Silva, R. M. S. Sousa, M. L. Jimeno, F. Blanco, I. Alkorta and J. Elguero, *Magn. Reson. Chem.*, 2008, **46**, 859.
15 F. Blanco, I. Alkorta and J. Elguero, *Magn. Reson. Chem.*, 2007, **45**, 797.
16 P. M. Mancini, G. G. Fortunato and L. R. Vottero, *J. Phys. Org. Chem.*, 2005, **18**, 336.
17 (*a*) S. E. Denmark and A. Thorarensen, *Chem. Rev.*, 1996, **96**, 137; (*b*) S. E. Denmark, B. S. Kesler and Y.-C. Moon, *J. Org. Chem.*, 1992, **57**, 4912; (*c*) S. E. Denmark, C. J. Cramer and J. A. Sternberg, *Helv. Chim. Acta*, 1986, **69**, 1971; (*d*) S. E. Denmark, Y.-C. Moon and C. B. W. Senanyake, *J. Am. Chem. Soc.*, 1990, **112**, 311.
18 (*a*) R. S. Paton, J. L. Mackey, W. H. Kim, J. H. Lee, S. J. Danishefsky and K. N. Houk, *J. Am. Chem. Soc.*, 2010, **132**, 9335; (*b*) N. Çelebi-Ölçüm, D. H. Ess, V. Aviyente and K. N. Houk, *J. Org. Chem.*, 2008, **73**, 7472.
19 J. E. Baldwin, *J. Chem. Soc., Chem. Commun.*, 1976, 734.
20 (*a*) C. O. Kappe and A. Stadler, *Microwaves in Organic and medicinal Chemistry*, Wiley-VCH, Weinheim, 2005; (*b*) *Microwaves in Organic Chemistry*, ed. A. Loupy, Wiley-VCH, Weinheim, 2nd edn, 2006.
21 (*a*) "How often have I said to you that when you have eliminated the impossible, whatever remains, however improbable, must be the truth?" A. Conan Doyle, The Sign of Four; (*b*) "It is an old maxim of mine that when you have excluded the impossible, whatever remains, however improbable, must be the truth". A. Conan Doyle, The Adventure of the Beryl Coronet.
22 C. Schweitzer and R. Schmidt, *Chem. Rev.*, 2003, **103**, 1685.
23 Although experimentally eliminated we have calculated the reaction *via* triplet [6-31G(d)+EtOH(PCM)]. Compound **4** in the ground state rotates about the N–C bond to yield **4′** which lies 2.6 kJ mol^{-1} higher in energy with a barrier of 19.1 kJ mol^{-1} (this process is preferred to the **4** → **4T**→**4′T**). Excitation of **4′** leads to **4′T** that, without barrier, affords intermediate **INT4** of Fig. 16. From **INT4** the reaction proceeds to **5** with a barrier of 35.6 kJ mol^{-1}.

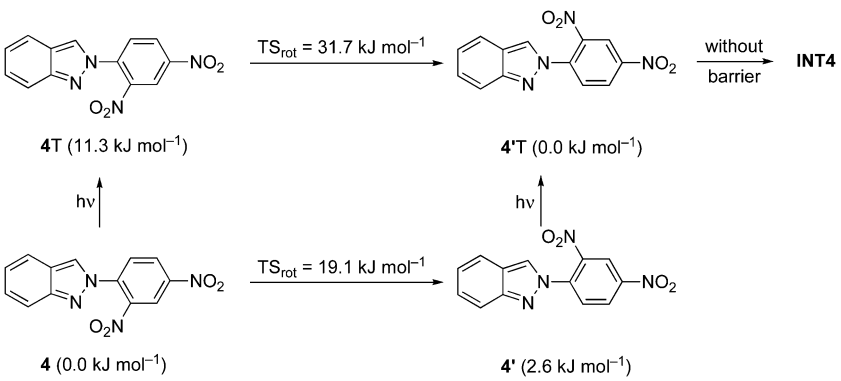

24 H. W. Heine, G. J. Blosick and G. B. Lowrie, *Tetrahedron Lett.*, 1968, **9**, 4801.
25 J. A. Sousa, J. Weinstein and A. L. Bluhm, *J. Org. Chem.*, 1969, **34**, 3320.
26 R. Bauernschmitt and R. Ahlrichs, *Chem. Phys. Lett.*, 1996, **256**, 454.
27 See for example: (*a*) T. Vreven, F. Bernardi, M. Garavelli, M. Olivucci, M. A. Robb and H. B. Schlegel, *J. Am. Chem. Soc.*, 1997, **119**, 12687; (*b*) N. Yamamoto, T. Vreven, M. A. Robb, M. J. Frisch and H. B. Schlegel, *Chem. Phys. Lett.*, 1996, **250**, 373; (*c*) F. Bernardi, A. Bottini, J. J. W. McDougall, M. A. Robb and H. B. Schlegel, *Faraday Symp. Chem. Soc.*, 1984, **19**, 137.
28 Oxford Diffraction, *CrysAlis CCD and CrysAlis RED. Versions (1.171.34.9)*, Oxford Diffraction Ltd, Abingdon, Oxfordshire, England, 2009.

 This journal is © The Royal Society of Chemistry and the Centre National de la Recherche Scientifique 2013

Published on 01 May 2013. Downloaded by Fudan University on 31/05/2013 12:55:02.

29 M. C. Burla, R. Caliandro, M. Camalli, B. Carrozzini, G. Cascarano, L. De Caro, C. Giacovazzo, G. Polidori and R. Spagna, *J. Appl. Crystallogr.*, 2005, **38**, 381.
30 G. M. Sheldrick, *SHELXS97 and SHELXL97*, University of Göttingen, Germany, 1997.
31 A. L. Spek, *J. Appl. Crystallogr.*, 2003, **36**, 7.
32 L. J. Farrugia, *J. Appl. Crystallogr.*, 1997, **30**, 565.
33 C. F. Macrae, I. J. Bruno, J. A. Chisholm, P. R. Edgington, P. McCabe, E. Pidcock, L. Rodríguez-Monge, R. Taylor, J. van de Streek and P. A. Wood, *J. Appl. Crystallogr.*, 2008, **41**, 466.
34 (*a*) C. Lee, W. Yang and R. G. Parr, *Phys. Rev. B*, 1988, **37**, 785; (*b*) R. G. Parr and W. Yang, *Density-Functional Theory of Atoms and Molecules*, Oxford, New York, 1989.
35 (*a*) A. D. Becke, *Phys. Rev. A: At., Mol., Opt. Phys.*, 1988, **38**, 3098; (*b*) W. Kohn, A. D. Becke and R. G. Parr, *J. Phys. Chem.*, 1996, **100**, 12974; (*c*) A. D. Becke, *J. Chem. Phys.*, 1993, **98**, 5648.
36 (*a*) W. J. Hehre, L. Radom, P. v. R. Schleyer and J. A. Pople, *Ab Initio* Molecular Orbital Theory, Wiley, New York, 1986, p. 76; (*b*) R. Ditchfield, W. J. Hehre and J. A. Pople, *J. Chem. Phys.*, 1971, **54**, 724; (*c*) W. J. Hehre, R. Ditchfield and J. A. Pople, *J. Chem. Phys.*, 1972, **56**, 2257.
37 M. J. Frisch, G. W. Trucks, H. B. Schlegel, G. E. Scuseria, M. A. Robb, J. R. Cheeseman, G. Scalmani, V. Barone, B. Mennucci, G. A. Petersson, H. Nakatsuji, M. Caricato, X. Li, H. P. Hratchian, A. F. Izmaylov, J. Bloino, G. Zheng, J. L. Sonnenberg, M. Hada, M. Ehara, K. Toyota, R. Fukuda, J. Hasegawa, M. Ishida, T. Nakajima, Y. Honda, O. Kitao, H. Nakai, T. Vreven, J. A. Montgomery, Jr., J. E. Peralta, F. Ogliaro, M. Bearpark, J. J. Heyd, E. Brothers, K. N. Kudin, V. N. Staroverov, R. Kobayashi, J. Normand, K. Raghavachari, A. Rendell, J. C. Burant, S. S. Iyengar, J. Tomasi, M. Cossi, N. Rega, J. M. Millam, M. Klene, J. E. Knox, J. B. Cross, V. Bakken, C. Adamo, J. Jaramillo, R. Gomperts, R. E. Stratmann, O. Yazyev, A. J. Austin, R. Cammi, C. Pomelli, J. W. Ochterski, R. L. Martin, K. Morokuma, V. G. Zakrzewski, G. A. Voth, P. Salvador, J. J. Dannenberg, S. Dapprich, A. D. Daniels, Ö. Farkas, J. B. Foresman, J. V. Ortiz, J. Cioslowski and D. J. Fox, *GAUSSIAN 09 (Revision A.1)*, Gaussian, Inc., Wallingford, CT, 2009.
38 (*a*) S. Miertus, E. Scrocco and J. Tomasi, *Chem. Phys.*, 1981, **55**, 117; (*b*) B. Mennucci and J. Tomasi, *J. Chem. Phys.*, 1997, **106**, 5151; (*c*) R. Cammi, B. Mennucci and J. Tomasi, *J. Phys. Chem. A*, 2000, **104**, 5631.
39 J. W. McIver Jr. and A. K. Komornicki, *J. Am. Chem. Soc.*, 1972, **94**, 2625.
40 (*a*) R. Ditchfield, W. J. Hehre and J. A. Pople, *J. Chem. Phys.*, 1971, **54**, 724; (*b*) M. J. Frisch, J. A. Pople and J. S. Binkley, *J. Chem. Phys.*, 1984, **80**, 3265.
41 (*a*) R. Ditchfield, *Mol. Phys.*, 1974, **27**, 789; (*b*) F. London, *J. Phys. Radium*, 1937, **8**, 397.
42 R. F. W. Bader, *Atoms in Molecules: A Quantum Theory*, Clarendon Press, Oxford, 1990.
43 P. L. A. Popelier, *Atoms in Molecules. An introduction*, Prentice Hall, Harlow, England, 2000.
44 T. A. Keith, 11.10.16 ed., *TK Gristmill Software*, 2011, http://aim.tkgristmill.com.